G. Rodriguez, S. Gilbertson, S.W. Vincent, and S.I. Jackson.
"Fiber Bragg Grating Sensors and Their Sensitivity to Changes in Detonation Velocity Across Interfaces."
In Proceedings of the 14th International Detonation Symposium, Office of Naval Research, pp. 264–265 (Office of Naval Research, 2015).

Fiber Bragg Grating Sensors and Their Sensitivity to Changes in Detonation Velocity across Interfaces

George Rodriguez[*], Steve M. Gilbertson[*], Samuel W. Vincent[#] and Scott I. Jackson[#]

[*]Materials Physics and Applications Division
Los Alamos National Laboratory, Los Alamos, NM, 87545

[#]Weapons Experiments Division
Los Alamos National Laboratory, Los Alamos, NM 87545

Abstract. Measuring detonation front position and velocity has been demonstrated using an all-optical chirped fiber Bragg grating (CFBG) approach with the ability to detect velocity changes across material interfacial boundaries. An experiment conducted with a cylindrical rate stick consisting of multiple high explosive (HE) segments of PBX 9501, Composition B, TNT, PBX 9407, PBX 9502, and finally inert PMMA. Spatial and temporal resolution was determined by comparing the measured detonation front position and velocity changes at interfaces by using long gratings (100 mm) with low spatial resolution and short (10 mm) gratings with high spatial resolution. A streak camera diagnostic independently validated all grating measurements. The gratings showed that the measurement resolution of unsteady detonation phase velocities increased with the high spatial resolution gratings. We attained a spatial resolution of 46 μm using the higher resolution 10 mm gratings. The spatial resolution is dependent on the vertical dynamic range of the 8-bit oscilloscope recording system, and it is expected to be below 10 μm should 12-bit recorders be used. Additionally, a decaying shock driven into the PMMA segment provided a measure of the minimum internal fiber pressure required for prompt grating destruction and accurate shock wave velocity measurement. This critical pressure was calculated to be approximately 2.1 GPa.

Introduction

Fiber Bragg grating (FBG) sensors are proving to be a valuable diagnostic for detonation and shock diagnostics.[1,2,3,4] They provide very good detonation and shock tracking performance when compared to other established methods such as electrical pins, optical streak camera recording, or velocimetry. They are relatively simple to field, offer a continuous measurement record, and do not need line-of-sight optics (such as in imaging or laser velocimetry) for operation. These sensors can be attached to inert and high explosive (HE) materials as surface or embedded probes, and because they operate in detonation and/or shock environments, their versatility makes them attractive as dynamic sensors in detonation and shock events of materials that are otherwise problematic to diagnose using surface-only probes. At Los Alamos, we have applied the technology to develop a diagnostic baseline for both HE detonation and shock velocity measurements. We

have previously reported on the accuracy of the approach for detonation front measurements by comparing with electrical pin data from rate stick measurements.[2,3,5] However, detailed questions about the resolution of the approach remained. Therefore, in this paper, we establish confidence levels in the approach by performing measurements that attempted to determine spatio-temporal resolution. The detonation and shock front measurements described here were aimed at quantifying resolution by comparison of several chirped FBG (CFBG) sensors with a high-resolution complementary diagnostic: an imaging streak camera. We chose an experimental test case where the detonation velocity was expected to vary rapidly, such as in a situation across interfacial boundaries where multiple segments of a rate stick was comprised of various HE formulations. In addition to measurements along the length and across interfaces of the HE portions, we also tested detonation-to-shock tracking across an HE/inert material interface by placing a piece of acrylic plastic at the end of the HE run. We used multiple CFBG sensors on this test with varying lengths and spatial wavelength chirp to determine the resolution of each type. Below we describe the methods of this test that yielded our results.

Methods

The technique of CFBG detonation front velocity measurements relies on technology originally developed for the telecommunications industry. A diagram of the principle of operation is shown in Figure 1(a). The detonation velocity detection system was described in detail elsewhere[2], and we give a brief description here. Our light source was an amplified spontaneous emission (ASE) source covering the C-band from 1525 nm to 1565 nm. Light launched from the ASE source into a single-mode fiber and directed to a 3-port circulator. The circulator directs light to a chirped fiber Bragg grating (CFBG) sensor. The CFBG was a linearly chirped grating written along some length of the fiber and with maximum reflectivity in the C-band. Reflected light return from the grating was directed through the circulator to the detector. A variable attenuator controlled the optical power to the gratings is so as not to saturate the detectors. All of the CFBG channels came integrated into two, four-channel chassis boxes from Timbercon Inc. Each channel inside the chassis box contained a 10% power tap for monitoring the spectrum of the returning light of the CFBG and a DC-coupled 50-Ohm output, 250-MHz InGaAs photodetector. The detectors yield a total temporal resolution limit of 4 ns. The signal from the 10% tap was sent to a fiber-based 512-element linear diode array spectrometer to characterize the spectrum of each grating before the detonation. The CFBGs send the light return power (typically 1 mW or 0.0 dBm) to the chassis box, which then outputs an electrical signal to a transient digitizer for recording with an oscilloscope. The recording bandwidth was 1 GHz and the sampling rate was 5 GSamp/s. With this setup, up to 8 CFBG sensors fieldable onto a single experiment with the capability of upgrading the number of channels only limited by the amount of light present in the ASE source. In theory, the number of channels may be as large as possible by simply using multiple ASE sources.

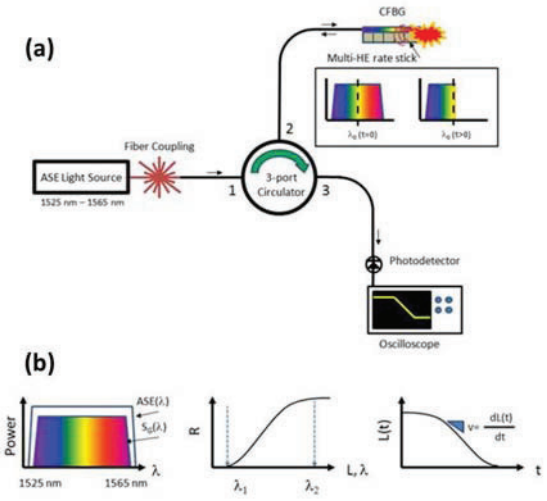

Fig. 1. (a) Chirped fiber Bragg (CFBG) detonation detection system. (b) The response functions for detonation measurements. The left panel shows the total reflected spectrum and ASE source. The center panel shows the total reflected light intensity ($R(t)$) as a function of wavelength and grating length. The right panel shows the length as a function of time of the grating as it is destroyed by a detonation front.

The CFBG was placed in direct contact with the HE and as the detonation wave travels along the length of the CFBG. As the HE detonation wave travels along the length of the sensor, the fiber's index of refraction is first modified by the intense shock driven into the fiber by the adjacent high-pressure detonation products as the wave propagates axially along the grating's length. In rapid succession, the grating is consumed by the high temperatures and pressures associated with this event. Shock-processed portions of the grating no longer transmit/reflect light due to substantial modification to the local index of refraction and damage of the grating structure. Once a segment of the grating is destroyed, that portion of the reflected spectrum is no longer present thereby causing the total light return signal to decrease. Figure 1(b) shows how the experimentally obtained oscilloscope trace of voltage versus time is transformed into a plot of length versus position. The center frequency of the grating reflection was ~1550 nm and the reflection bandwidth was less than the bandwidth of the ASE source. We selected of only the flattest portion of the spectrum for the experiments. While this was not necessary, it simplified the data analysis procedure. The time-dependent reflected intensity, $R(t)$, is proportional to the integral of the returning light spectrum of the grating. In general, the integrated light return voltage signal is given[2] by:

$$R(t) = a \int_{\lambda_1}^{\lambda_2(t)} S_G(\lambda) ASE(\lambda) d\lambda \,, \tag{1}$$

where a is a normalization constant, $S_G(\lambda)$ is the reflected spectrum from the grating, $ASE(\lambda)$ is the ASE light source spectrum, and λ_1 and λ_2 are the lower and upper wavelength limits, respectively. When the gratings are encoded with the chirp, the length to wavelength relationship is linear meaning $R(t)$ is proportional to both length, L, and wavelength, λ, provided the ASE light source spectrum can be assumed to be flat. Once $R(t)$ versus L is known, a look-up-table is created to map the experimentally obtained $V(t)$ signal from the oscilloscope traces to a grating length, L, versus time. The time derivative of this curve yields the detonation velocity along the length of the fiber.

Results

For this experiment, a multi-HE rate stick comprised of five types of HE and an inert PMMA segment was used to test the effectiveness at measuring detonation velocities from three types of CFBGs with different linear chirp rates. The goal was to measure the spatial resolution capabilities of the gratings. In one case, short gratings with a quick variation of reflected wavelength versus length placed at the interfaces between each HE segment. This was compared with long gratings having a slower variation of reflected wavelength versus length but able to cover several interfaces with a single grating. Figure 2(a) shows a schematic for how the gratings mounted on the rate stick. The HE charges were first marked with right angle square ruler to indicate the linear placement position of the gratings. The effect of misaligned non-normal position of the gratings with respect to the burn front was not considered, but it could potentially lead to phase velocity error depending on the angular misalignment during placement. Detailed studies of such effects should be a subject of future investigation. The rate stick itself consisted of 5 types of HE (PBX 9501, Composition B, TNT, PBX 9407, and PBX 9502) followed by an inert PMMA segment. Each segment was 25.4 mm long and 12.7 mm in diameter. An RP-1 detonator initiated the rate stick. The test diagnostics consisted of five 10-mm-long CFBGs, a 70-mm-long CFBG, and a 100-mm-long CFBG. We mounted the longer two gratings so that they overlapped each other for redundant data acquisition. All of the CFBGs were glued in place (M-bond 200 epoxy) as shown in Figure 2. The gratings were attached at slightly different azimuth angles to avoid fiber cable interference. The spectra for the gratings are shown in figure 2(b) for the 10-mm CFBGs and (c) for the 70-mm and 100-mm CFBGs. In all cases, the spectra are relatively flat. The chirp of each CFBG was measured before and after attachment to the HE rate stick using an optical backscatter reflectometer. The measured chirp values for the 10-mm gratings were all ~3.5 nm/mm, 0.49 nm/mm for the 70-mm gratings, and 0.35 nm/mm for the 100 mm grating.

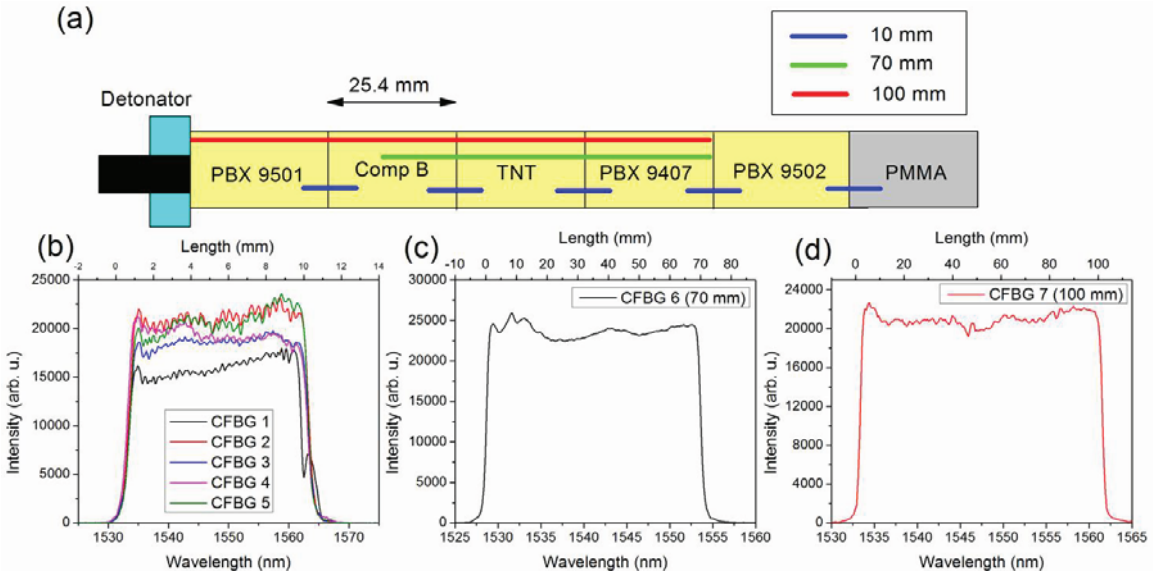

Fig. 2. (a) Illustration of the multi-HE rate stick experiment. Each segment was equal in length, and gratings of various sizes given by the blue, green, and red line segments covered the interfaces. The reflected spectrum of each grating showing the overall flat-topped nature are shown for the (b) 10 mm gratings, (c) the 70 mm (black line), and (d) the 100 mm (red line).

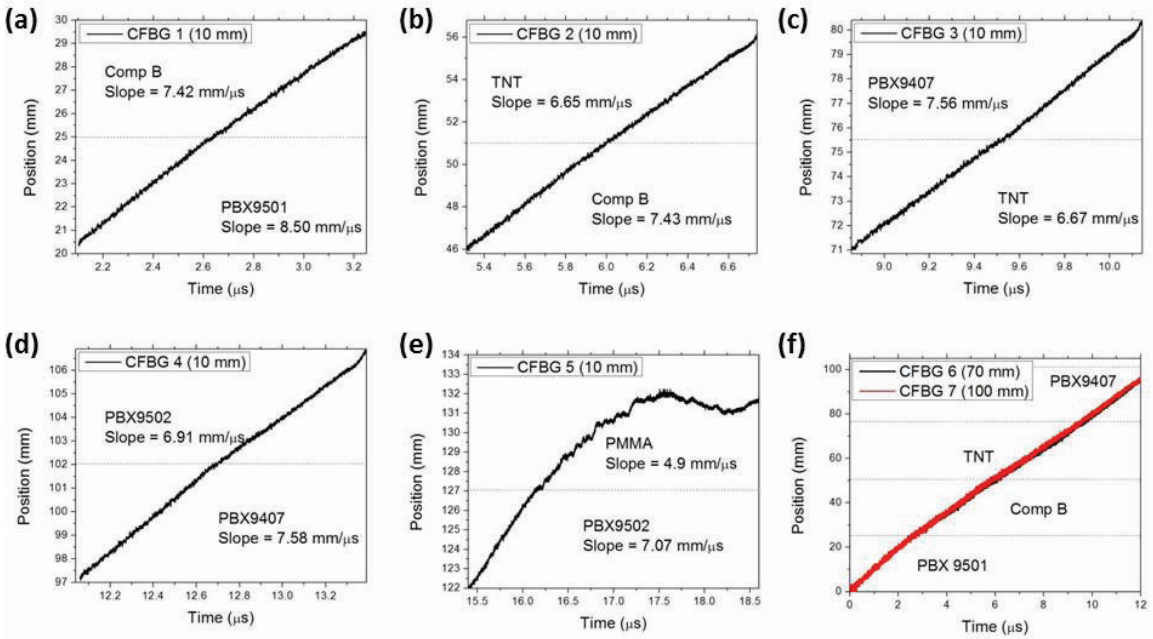

Fig. 3. The measured velocity across the interfaces of each HE segment for the 10 mm gratings. The type of HE and the velocity are indicated. (f) The measured velocity across the interfaces for the 70 mm (black) and 100 mm (red) gratings. The two curves are very similar and lie on top of each other. The horizontal lines indicate the locations of the HE interfaces in all graph panels (a)-(f).

Figure 3 shows the experimental data. The 10 mm gratings are shown in 3(a)-(e) while the 70-mm and 100-mm gratings are both shown in 3(f). In all panels of Figure 3, the horizontal dashed lines represent the interfaces of the different HE segments. A discontinuity occurs at the interfaces in (a)-(e) due to velocity of the detonation front changing as it enters a new HE segment. These changes are not as pronounced in the longer gratings (Figure 3(f)) however. We can attribute this to the increased spatial resolution afforded by the shorter gratings. Additionally, in (e) the inert PMMA segment shows a shock wave launched into the material, as opposed to a detonation wave, as expected. The nature of the signal is indicative of an attenuating pressure shock that partially disrupts the sensor as opposed to destroying it after a few mm of propagation into the sample. A label in each plot indicates the average detonation velocity across the sensor for each HE segment. For the 10-mm CFBGs, the average detonation velocity was determined by performing a linear fit to 4.75 mm of the position data for each material segment (approximately 5 mm of each 10 mm CFBG grating was located on separate HE types). The velocities are within good agreement of accepted values[6] with differences stemming from the small diameters of the rate stick not allowing for maximized detonation velocity.

It is important to note that the dynamic range of the oscilloscope's vertical scale limited the overall spatial resolution the gratings. The maximum linear photodetector output is 2 Volts DC. The oscilloscopes used in this experiment were 8-bit. Therefore, the smallest resolvable incremental voltage difference is ~7.8 mV (*i.e.*, 2 V/2^8). An incremental voltage change of 7.8 mV yields an ultimate spatial resolution from the oscilloscope (Δs_{osc}) of ~39 μm for the 10 mm gratings and ~390 μm for the 100 mm grating. The real experimental spatial resolution was worse than this, due to the noise of the scope channels inherent in the system and stemming from the 250 MHz photodetectors. The scope itself had a sample rate of 2.5 GSamp/s allowing the data to be oversampled. Averaging the data by 10 points to take advantage of the oversampling reduced the noise floor to ~5 mV. Resolution from such a noise level, which we call Δs_{noise} and with the ultimate resolution from the scope, we find an experimentally obtained spatial resolution $\Delta S=(\Delta s^2_{osc} + \Delta s^2_{noise})^{1/2}$ of ~46 μm for the 10 mm grating and nearly 460 μm for the 100 mm grating. Table 1 shows the results of the spatial resolution and temporal resolution for an 8 mm/μs detonation wave measured from each of the grating lengths. By using detectors with less noise and scopes with higher dynamic range, a significant improvement to spatial resolution is expected. For example, a 10-bit scope would be able to resolve a voltage change of 1.9 mV while the 12-bit scope can resolve 0.5 mV. These correspond to ultimate resolutions of 98 μm (9.8 μm) and 24 μm (2.4 μm), respectively for the 100 mm (10 mm). This represents a significant improvement over the resolution of the 8-bit scopes and is being implemented in future experiments.

Table 1. List of the fiber lengths and chirps used in this experiment along with measured temporal and spatial resolutions with 8-bit recording. 10-bit and 12-bit based oscilloscopes vastly improve these numbers.

Length (mm)	Measured Chirp (nm/mm)	Temporal Resolution (ns)	Spatial Resolution (μm)
100	0.35	57	460
70	0.49	40	322
10	3.5	5.8	46

In addition to the CFBGs, an imaging streak camera (Cordin Model 132) simultaneously recorded the position of the detonation front versus time. An external light source front illuminated the charge. The charge had a polished flat facet to allow for specular light reflection off the facet surface using an argon flash light source.[7] Light collected off the flat surface reflection was imaged on to the streak camera. The explosively-driven argon flash contained light intensity of sufficient brightness that overwhelmed the intensity produced by explosive product self-light from the charge. Figure 4(a) shows the streak camera image with the static image at the top and the dynamic data on the bottom. Figure 4(b) shows the results of extracting the position vs. time data. The streak camera data (black solid line) is shown superimposed with the 10 mm gratings appearing

approximately every 25 mm (short solid colored segments). The agreement between the streak camera data and gratings is excellent with ~1% error in the measured velocities. This error could come from discrepancies in the measured lengths of each grating. Also shown in Figure 4(b) are the data sets for the longer CFBGs. These are the green dotted lines (100 mm) and purple dotted line (70 mm). The sets are difficult to distinguish because they lie on top of each other so well. The data agrees well with both the 10 mm grating data and the streak camera data. Since the spatial resolution of the two longer gratings was worse than the smaller gratings, we do not expect to see as small of changes in the velocity for the long gratings. However, since they are long enough to cover several segments of the multi-HE rate stick, we can compare the overall subtle changes seen in the streak camera data to the grating data. The results here are also in agreement with the accepted values.[6] There is a larger error in the 100 mm grating as compared to the streak camera data at the very beginning which we can attribute to the grating being in close proximity to the detonator. This effect quickly disappears and the grating data and streak camera show agreement after the first 7-8 mm. The effect was not observed in the 70 mm grating.

Finally, in the PMMA sample segment, the CFBG data diverges heavily from the streak camera data. The spatial location where the divergence begins is ~5 mm away from the PBX9502 interface inside the sample at t~17.5μs (Fig. 4(b)). This behavior is indicative of the minimum pressure where the CFBG is no longer promptly destroyed. The PMMA shock velocity at this point as given by the streak camera data is ~4.22 mm/μs. Using the Hugoniot relations $U_s=c_0+su_p$ and $P=\rho_0 U_s u_p$, and solving for P after eliminating u_p yields the pressure in the HE. In the above equations, U_s is the shock velocity from the streak camera data, u_p is the particle velocity, ρ_0 is the uncompressed density, c_0 is the speed of sound in the bulk material, and s is a parameter describing the slope of the shock Hugoniot. For PMMA, s=1.816, c_0=2.260 mm/μs, and ρ_0=1181 kg/m^3. Using the shock Hugoniot[8], we estimate the pressure in the PMMA as 5.38 GPa at the point that the two datasets diverge. The pressure and

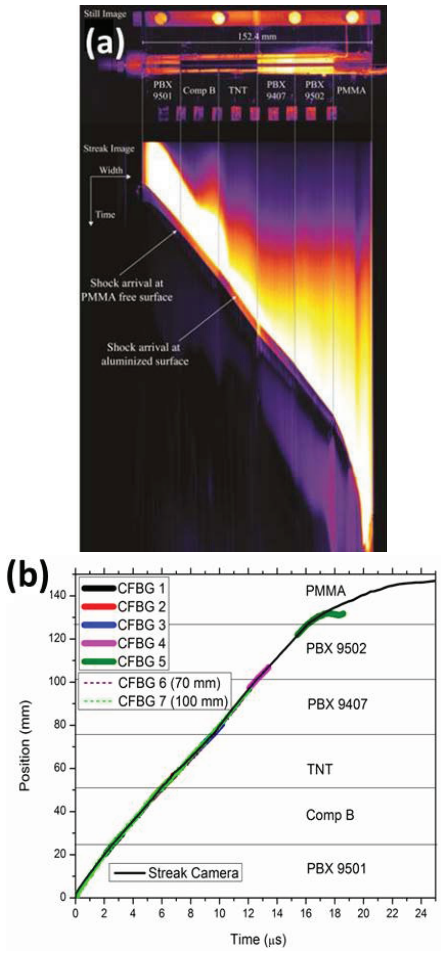

Figure 4(a) Image of the static (top) and dynamic (bottom) streak camera measurement. The locations of the HE interfaces are shown as the vertical lines. (b) Comparison of the position versus time data of the 10 mm gratings (small solid segments), 70 mm grating (purple dotted line) and 100 mm grating (green dotted line) to the streak camera velocity measurement taken from (a) (black solid line).

particle velocity within the fiber itself will be different from the PMMA however due to the impedance mismatch of the two materials. We assume the high-pressure PMMA drives a shock laterally into the adjacent fiber fused silica fiber and we calculate the pressure induced in the fiber at the critical velocity. The post-shock state resulting from the interaction of the two adjacent materials was solved by assuming impedance

matching of the pressure and particle velocity within the two materials at the interface. The interaction of these two materials gives the effect that the PMMA will expand with decreased pressure and increased particle velocity along an isentrope. Conversely, the fused silica of the fiber is compressed along a shock adiabat. Arriving at an exact PMMA isentrope is difficult but we can take advantage of the fact that the isentrope tracks the Hugoniot for small expansions and thus we can assume that the previously calculated Hugoniot will represent the PMMA expansion. Solving for the intersection between two Hugoniot curves for both PMMA and the fused silica fiber gives a pressure of 2.05 GPa at the point that the fiber is destroyed. Pressures above this limit yield destruction of the grating and an accurate measurement of the detonation/shock velocity while pressures below show a decaying shock wave propagating into the grating. The streak camera data (black curve in Figure 4) shows that the shock continued beyond what the grating was capable of measuring. Measured values of velocity are no longer valuable below these pressures since, although information on the pressure can clearly be deduced from the shape of the curve, ambiguities in the true behavior of the shock wave are present since the grating is not instantaneously destroyed and instead retains its mechanical integrity.

Conclusions

A robust all optical method using CFBGs to measure detonation wave velocity was developed. Using gratings with longer lengths but lower spatial resolution accurately mapped the detonation front in a multi-shot rate stick. Shorter gratings with higher resolution were shown to more accurately measure small changes in the velocity of detonation waves at the interfaces of different types of HE. This however comes at the sacrifice of only measuring a smaller portion of the HE itself. The overall spatial resolution offered by the 10 mm gratings was 46 μm. An increase in the dynamic range of the scopes and detectors could significantly reduce this. Due to the flexibility of the gratings, measurements can be made on more complex and even curved geometries.[2] Scaling up the number of channels could allow more gratings to be installed on the same HE shot to allow higher resolution and possibly even three dimensional tracking of detonation waves across the entire volume of the HE. We also believe that these results are useful for those considering use of CFBGs for card gap tests with CFBGs showing the ability to track across multiple interfaces.

Acknowledgements

This work was supported by the DOE/NNSA Leda project at Los Alamos National Laboratory under the auspices of the U.S. Department of Energy for Los Alamos National Security, LLC, Contract No. DE-AC52-06NA25396.

References

1. Udd, E., and Benterou, J., “Improvements to High-Speed Monitoring of Events in Extreme Environments using Fiber Bragg Grating Sensors” *SPIE*, Vol. 8370, 83700L, 2012.

2. Rodriguez, G., Sandberg, R. L., McCulloch, Q., Jackson, S. I., Vincent, S. W., and Udd, E., “Chirped Fiber Bragg Grating Detonation Velocity Sensing” *Rev. Sci. Instrum.*, Vol. 84, 015003, 2013.

3. Rodriguez, G., Sandberg, R. L., Jackson, S. I., Vincent, S. W., Dattelbaum, D. M., McCulloch, Q., Martinez, R. M., Gilbertson, S. M., and Udd, E., “Fiber Bragg Grating Sensing of Detonation and Shock Experiments and Los Alamos National Laboratory” *SPIE*, Vol. 8722, 8722O4, 2013.

4. Shafir, E., Zilberman, S., Ravid, A., Glam, B., Appelbaum, G., Fedotov Gefen, A., Saadi, Y., Shafir, N., and Berkovic, G., “Comparison of FBG Responses to Static and Dynamic Pressures” *SPIE*, Vol. 9157, 915713, 2014.

5. Rodriguez, G., Sandberg, R. L., Jackson, S. I., Gilbertson, S. M., and Udd, E., “Fiber Bragg Sensing of High Explosive Detonation Experiments at Los Alamos National Laboratory”, *J. Phys. Conf. Ser*, Vol. 500, 142030, 2014.

6. Gibbs, T. R., and Popolato, A., "LASL Explosive Property Data" Los Alamos Scientific Laboratory Series on Dynamic Material Properties, University of California, Berkeley, 1980.

7. Davis, W. C., Salyer, T. R., Jackson, S. I., and Aslam, T. D., "Explosive-Driven Shock Waves in Argon" *Proceedings of the 13th International Detonation Symposium*, pp. 1035–1044, Norfolk, VA, July 2006.

8. Boslough, M. B., and Asay, J. R., "Basic Principles of Shock Compression", in *High Pressure Shock Compression of Solids*, edited by J. R. Asay and M. Shahinpoor, pp. 7-42, Springer-Verlag, New York, 1993.

Question

Paul Wilkins, LLNL
Does the fiber break under shock compression or upon the release wave after shock loading?

Reply by George Rodriguez
In set of separate flyer-plate impact shock driven experiments with short (~1-mm long) fiber Bragg grating sensors, initial data evidence suggests that sensors withstand the initial compression as the shock transits the length of the grating, and then fractures during the release some time afterwards. Studies are in their early stages showing that the short fiber Bragg sensors withstand but compression ~5 GPa, but then they fracture in release state after some equilibration time. Results are preliminary, but seem to show that they are stronger in compression than in tension.

Matthew Biss, ARL
How do the spatial and temporal scales of the fiber compare to the streak camera?

Reply by Scott Jackson and George Rodriguez
Both diagnostics offer scalable resolution and field of view. The streak camera resolution is scalable depending on the magnification used. The film width is 70mm and we scan it in at 6400 dpi. When using this process, we do not resolve the film grains. Thus, in theory, we could then vary the magnification to the limit of the field lensing resolution to achieve the highest resolution possible. We could also scan in the film at higher resolution until we resolve the grain size. The CFBG resolution is also scalable depending on the chirp and detector response time, it can also be scaled for the resolution needed for each application. In the configuration fielded, the streak camera resolution was ~140 μm. Therefore the streak camera had resolution roughly the twice the spatial resolution that the 10 mm CFBGs (46 μm) and 3.3 times better the resolution than the 100 mm CFBGs (460 μm). However, should a 12-bit recording digitizer be used, the CFBG system would have a resolution comparable or even better than the streak camera under the same conditions, and the limitation in the CFBG approach may then be limited by the spatio-temporal smearing introduced by the photodetectors used (250 MHz).

Question

Aubrey Farmer, NAWC WD
Are the fiber Braggs affected by temperature?

Reply by George Rodriguez
Yes. Temperature related effects are produce a linear shift in the reflection spectrum of the grating. A typical temperature induced shift in a fused silica fiber Bragg gratings is $(\Delta\lambda/\Delta T) \approx +0.03$ nm/°C. The spectrum shifts slightly to longer wavelength with increasing temperature, an effect that must be taken into account when performing measurements. For example, a grating installed on a sample heated to 100° C will shift the entire grating spectrum 2.25 nm to longer wavelength over its room temperature spectrum. We find that in heated high-explosive experiments, the spectrum of the grating should be measured as close as possible to final temperature before execution of the shot to account for calibration changes from temperature changes in the grating or sample.

Question

H. Keo Springer, LLNL

Do you plan any more experiments to characterize the threshold FBG/Fiber crush pressure as follow-up to PMMA experiments? What would be influence of fiber material sound speed on sensing sub-sonic (in fiber) deflagrations?

Reply by George Rodriguez
We have performed a small set of HE-driven Taylor wave and small bore gas gun-driven plate-impact experiments with very short 1-mm-long fiber Bragg gratings serving as point-like pressure sensors that spectrally shift in response to the shock stress level. The fiber sound speed is important to interpreting the results. Because the fiber sensors used were 1-mm-long, an inherent equilibration time is observed (~180 ns) before the full length of the sensor is pressurized. We are currently planning a set of large bore gas-gun experiments where the pressure is uniform for a longer period that what has been done to date. We wish to resolve the full pressure dynamics during the loading, equilibration, and release. For detection of sub-sonic deflagrations, a separate fiber approach may have to be used. Recent coherent time domain approaches we developed to interrogate fiber Bragg gratings provide spectrum and length information directly, and it may be possible to distinguish HE induced pressure and/or temperature signatures separate from a run ahead sound wave traveling in the fiber. Another possible approach would be to use a distributed array of very short (0.5 mm long) gratings in series on a single fiber where each mini-grating can serve as point sensors rather a continuous approach such as a CFBG.

Question

James Ferguson, AWE
How much better can the resolution be made by increasing the width of the reflected spectrum?

Reply by George Rodriguez
Apart from increasing the vertical resolution of the recording system, spectrally encoding a larger spectral band on a chirped grating should increase spatial resolution in linear proportion to the bandwidth of the grating. Some of the longest chirped gratings to date are custom made 200 mm long gratings that cover both the C- and L-band (C: 1525-1565 nm, L:1570-1610 nm) portions of the telecommunications band. Choosing the appropriate broadband light source becomes a potential issue, but it should be possible to fit a larger band per unit length of grating. Ultimately, the intrinsic limit is the optical fiber Bragg reflection condition and the chirp rate necessary to achieve the desired bandwidth in a given length. We have not fully explored this approach, but we also believe that the resolution increase with this approach will not be much more than a factor of a few. We base our opinion on information that the 10-mm-long C-band CFBGs used in this experiment are some of the shortest available gratings capable of accommodating the C-band spectrum.